The flow past a flat plate of finite width

By J. W. ELDER
Geophysics Division, D.S.I.R., Wellington, New Zealand

(Received 8 February 1960)

An experimental study of the incompressible flow near the side edge of a finite flat plate at zero incidence is reported for the Reynolds number range 10^4 to 10^6, but comparison with data already published shows that the conclusions are quantitatively valid for Reynolds numbers up to 10^9. The laminar velocity field is everywhere convex and does not contain any secondary flow other than that of the normal diffusive growth of the layer, but has a logarithmic singularity at the edge where the stress is controlled by the local radius of curvature. The excess skin friction due to the edge is considerably greater than that given by calculations based on the Rayleigh approximation but agrees with a recent Pohlhausen calculation by Varley (1958). Near the edge the high stress and ease of momentum diffusion makes the flow very unstable and turbulent spots occur well upstream of the normal transition zone in the middle of the plate. The spots originate from a nearly point-like region at the edge of the plate and grow linearly in time at the same rate as ordinary turbulent spots to sweep out a narrow tongue of turbulent fluid near the edge until they merge with the normal transition zone. Within this tongue a weak secondary flow of Prandtl's second kind, driven by the anisotropic Reynolds stresses, begins to develop. In fully turbulent flow when the secondary flow is largely localized to within a few boundary-layer thicknesses of the edge the secondary flow velocities are everywhere less than 0·04 of the free-stream velocity. Nevertheless, the secondary flows from each of the side edges interact, regardless of the width of the plate, to increase the total drag coefficient by an amount 0·0004 which is independent both of the Reynolds number and the width of the plate except when it is very narrow. This simple result allows apparent discrepancies between various formulations of the drag coefficient of a finite plate to be reduced to less than $\pm 1\,\%$ S.D. Of these formulations Schoenherr's (1932) empirical relation agrees best with the present data.

1. Introduction

Here is an experimental study of certain three-dimensional boundary layers directed towards a knowledge of the laminar, transitional and turbulent flow over a flat plate of finite breadth and in particular to the flow near a side edge. Consider a thin rectangular plate of breadth B and thickness $T \ll B$ in the XOZ plane of the Cartesian frame $OXYZ$ in a uniform free stream of velocity U_1 parallel to OX, as shown in figure 1. Let the side edges $z = 0, B$ be rounded to some definite form so that the typical radius of curvature of the edge cross-section a is of order T and the leading edge of sufficiently slender elliptical form to avoid separation, except during studies of the fully turbulent flow when separation

and transition is encouraged by a leading edge of square form. The flow at section x will be determined by U_1, the kinematic viscosity ν, x, a and B. (The intensity of turbulence in the free stream will also be important but its effect will not be considered here.) Suitable dimensionless parameters are the Reynolds number $R = U_1 x/\nu$, δ/a and δ/B, where $\delta(x)$ is the boundary-layer thickness. Near the leading edge for laminar, transitional and turbulent flow the flow will be dominated by R. Further downstream where the boundary-layer thickness is no longer small compared with a or B the flow will be influenced by the form of the

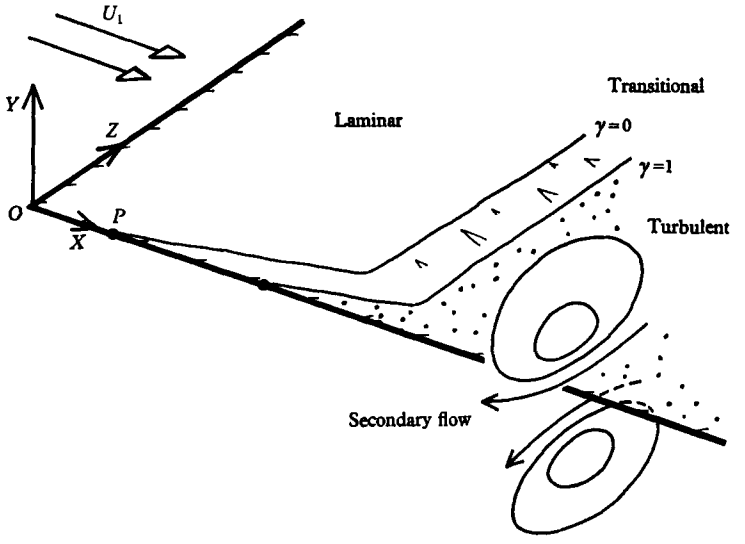

FIGURE 1. Diagram of the edge of a flat plate showing the Cartesian co-ordinate system, the laminar, transitional and turbulent flow areas and the form of the mean secondary flow streamlines.

body cross-section. Such effects arise near the side edges of the plate and will be found to be dominated by δ/a for laminar and transitional flow but by δ/B for turbulent flow. Initially the flow in the middle of the plate is unaffected by the presence of the edges, but for large values of δ/B when the boundary-layer thickness is comparable with the largest dimension of the body cross-section the entire flow field is influenced by the presence of the edges. For very large values of δ/B when the boundary-layer thickness is very much larger than B the flow is again almost everywhere independent of the form of the body cross-section. The present work is a study of the dependence of the various flow régimes on the above parameters. Briefly, as sketched in figure 1, these flow régimes, laminar, transitional and turbulent, will be found to succeed each other in the normal fashion except that near the edge (1) in the laminar zone the wall stress is very large, (2) transition to turbulence occurs very early and (3) the turbulent flow maintains a weak secondary flow. These effects are not unexpected.

In spite of a considerable amount of work in recent years on three-dimensional laminar boundary layers (Moore 1956) very little progress has been made for the present case where the boundary wall is everywhere parallel to the incident flow. The only full solution of such a flow is the calculation by Lighthill & Glauert

(1955) for the axisymmetric boundary layer on a circular cylinder. No detailed solution of the laminary boundary-layer flow near an edge has been given but two well-known approximations have been applied to the problem. The first is based on Rayleigh's (1911) method of obtaining a rough answer by assuming that momentum is convected everywhere at the speed of the free stream. Batchelor (1954) has applied the method to cylinders of arbitrary cross-section, while Howarth (1950) has given a detailed solution for the flow near the edge of a quarter-infinite plate. Lighthill & Glauert (1955) showed that the approximation is good only a long way downstream. The second approach is Varley's (1958) valuable calculation of the total drag for cylinders of arbitrary section by a Pohlhausen method.

The comparative stability of a laminar boundary layer over, say, a laminar jet is due to the restraining action of the wall. Near an edge it is to be expected that the restraint will be less than that distant from the edge so that disturbances will grow more quickly near the edge. In fact, after my experiments were completed, I found that there was already definite evidence in the literature to this effect. First, Murphy & Phinney (1951) to illustrate a paint method of indicating transition give a photograph showing the transition curve on a finite flat plate. Secondly, Tagori *et al.* (1955) have compared the position of transition as indicated by hot wires and the paint method by means of the flow over a semi-submerged plank. In both instances no particular significance was attached to the form of the transition curves. The curves show, near the edges, wedges of turbulent fluid growing downstream at an angle of 8–10° to the wall (as sketched by the lines $\gamma = 0$ and $\gamma = 1$ in figure 1) till they merge with the normal transition zone. This is similar to the so-called transverse contamination of a laminar flow studied by Charters (1943).

For practical reasons such as estimating the drag of ships it is desirable to make measurements of the frictional drag on flat plates due to the turbulent boundary layer at the largest possible Reynolds number, in which case it has been necessary to use rather narrow rectangular plates (Hughes 1954) when the drag coefficient may be influenced by the finite width of the plates. In 1954 Townsend predicted that the inequality of the normal Reynolds stresses in the turbulent layer would produce a secondary flow near the edge. The Reynolds equations for the turbulent layer on a finite flat plate for a fluid of density ρ, mean velocity (U, V, W) and fluctuating velocity (u, v, w) are

$$U\frac{\partial U}{\partial x} + V\frac{\partial U}{\partial y} + W\frac{\partial U}{\partial z} + \frac{\partial}{\partial y}\overline{uv} + \frac{\partial}{\partial z}\overline{wu} = -\frac{1}{\rho}\frac{\partial P}{\partial x} + \nu\left(\frac{\partial^2 U}{\partial y^2} + \frac{\partial^2 U}{\partial z^2}\right), \tag{1.1}$$

$$\frac{\partial}{\partial y}\overline{v^2} + \frac{\partial}{\partial z}\overline{vw} = -\frac{1}{\rho}\frac{\partial P}{\partial y}, \tag{1.2}$$

$$\frac{\partial}{\partial y}\overline{vw} + \frac{\partial}{\partial z}\overline{w^2} = -\frac{1}{\rho}\frac{\partial P}{\partial z}. \tag{1.3}$$

Consider a point (x_0, y_0, z_0) distant from the edge or by symmetry where $\overline{vw} = 0$ so that integrating (1.2) with respect to y,

$$-\rho\overline{v_0^2} = P_0 - P_1, \tag{1.4}$$

where P_1 is the pressure outside the layer and P_0, v_0 are evaluated at (x_0, y_0, z_0). Further, integrating (1.3) with respect to z,

$$\rho\int_{-\infty}^{z_0}\frac{\partial}{\partial y}\overline{vw}\,dz-\rho\overline{w_0^2}=P_0-P_1. \tag{1.5}$$

By (1.4), (1.5)
$$\int_{-\infty}^{z_0}\frac{\partial}{\partial y}\overline{vw}\,dz=\overline{w_0^2}-\overline{v_0^2}. \tag{1.6}$$

Near the wall $\overline{w_0^2}-\overline{v_0^2}\doteqdot 2\tau_0/\rho$ (Klebanoff 1954) where τ_0 is the skin friction. If $\overline{vw}$ is concentrated in a narrow strip of width b then $\partial\overline{vw}/\partial y$ will be of order $\tau_0/\rho b$. Within this strip the stress will not be parallel to the free stream and the high values of $\partial\overline{vw}/\partial y$ will induce rapid accelerations of the flow. Such a secondary flow is similar to that found in pipes of non-circular section and is a flow of Prandtl's second kind (1952). The mean streamlines of the secondary flow are sketched in figure 1.

2. The experimental method

The flow around a number of slender metal bodies was measured. The bodies were (1) flat plates of widths 2, 6, 22, 30 cm and thickness 0·16 cm and a similar plate of width 20 cm but with one edge chamfered to 10°, (2) rods of rectangular section 3·84 × 0·32 cm and 0·64 × 0·32 cm, called the 12:1 and 2:1 rods, and (3) a circular cylinder of diameter 0·59 cm. They were all 100 cm long with the leading edge shaped to the form of 8:1 ellipses or left square for turbulent flow. The corners of the side edges were rounded to a radius of 0·5 mm except for 0·15 mm on the chamfered plate. The bodies were supported from the rear so that the edge or axis of symmetry was near the tunnel centre line.

Most of the measurements were made in the 15 in. wind tunnel of the Cavendish Laboratory. The working section is 38 cm square and 200 cm long. Speeds from 30 to 1500 cm/sec are available. The total turbulence intensity is about 0·1 % at medium speeds. Above 300 cm/sec U_1 is obtained from a manometer operated across the contraction and at low speeds an anemometer is available in which the temperature of a 1 mm diameter wire, heated by a constant current, is determined by a thermocouple. The anemometers are calibrated by means of hot-wire measurements of phase in the periodic heat wake of a fine wire heated from the mains. Mean velocities were measured by either total head tube or hot-wire methods. No correction has been made for the finite size of the total head tube in relation to the boundary-layer thickness. Measurements of turbulent quantities were with hot wires of normal length 0·7 mm made from 2·5 μ Wollaston wire. The wire gives an output proportional to $2[\{1+(u/U)^{\frac{1}{2}}\}-1]$ rather than u/U but the difference is usually small. Further, it has been found that heat conduction and convection effects lead to serious errors if hot wires, run at 450 °K, are used closer than 1 mm from a thermally conducting plate in air. These effects limit the accuracy of measurements of skin friction using a hot wire to ± 10 % S.D. Records of the velocity trace were obtained from a photographic drum camera with a film speed up to 200 cm/sec and studies of transient behaviour were by means of a camera and a triggered oscilloscope.

The detection and direct measurement of mean secondary flow was performed with a vortameter (Truitt 1956). This is a very thin vane, normally 1×1 cm, mounted on a spindle so that the vane can rotate. When the spindle is pointed into the wind the vane remains stationary unless there is a component of vorticity parallel to the wind. Rotational speeds were determined stroboscopically.

Turbulent skin friction was determined by the surface-tube method developed by Preston (1954). Provided the surface tube of diameter d lies within the region of wall similarity there exists a relation,

$$d^2\Delta p/\rho\nu^2 = F(\tau_0 d^2/\rho\nu^2).$$

Δp is the pressure difference between the pressure in the surface tube and the local static pressure, and τ_0 is the skin friction. Preston determined the function F by experiment for tubes of inner to outer diameter ratio 0·6. Comparison of the results near an edge, for tubes of different diameter, show that reliable measurements can be made up to one tube diameter from the edge.

Some qualitative experiments were made in the 14 in. water flume of the Engineering Laboratory, Cambridge. A flat plate was immersed in the water in the flume and permanganate solution injected through a narrow slit 4 cm downstream of the leading edge (or more simply by merely sprinkling the plate with dye crystals). This dye later normally remained close to the wall as it was convected downstream but would be quickly broken up by any disturbance to the flow. The detailed motion of such disturbances and in particular that of turbulent spots was clearly revealed by the method.

Throughout this work I have used as a measure of the boundary-layer thickness δ, the distance measured normal to the wall at which the mean velocity $U = 0{\cdot}99U_1$. At first sight this would appear to be a difficult quantity to measure. It is found, however, that if the velocity profile is plotted on probability paper the outer part of the layer generally gives a straight line. This is found to cover a wide range of laminar and turbulent flows and δ can thus be found quite accurately from the straight line drawn through the outer experimental points. It is worth noting that for a laminar Blasius layer $\delta \doteqdot 5\,(\nu x/U_1)^{\frac{1}{2}}$, whereas for a turbulent layer on a flat plate δ varies from $0{\cdot}02x$ to $0{\cdot}01x$ over the range $R = 10^6$ to 10^9 (Schlichting 1955).

3. Laminar flow

The experimental velocity distribution

Figures 2 and 3 show the distribution of U on a plane x = constant, based on measurements with a 1 mm total head tube made at $x = 20$ cm, $R = 1{\cdot}06 \times 10^5$ for the flat plate of figure 2 and at $x = 37$ cm, $R = 7{\cdot}2 \times 10^4$ for the 2 : 1 rod of figure 3. It is important to notice, especially in comparison with the corresponding turbulent flows below, that the U-distributions are everywhere convex. This is strong evidence that there is no secondary flow other than the diffusive growth of the layer so that even within the boundary layer the flow is nearly unidirectional.

The boundary-layer thickness at the edge of the flat plate is only 0·35 of its value distant from the edge δ_∞ so that as the edge is approached the local skin friction rises. The local skin friction coefficient c_f is defined in terms of the wall

stress τ_0 by $\tau_0 = \frac{1}{2}\rho U_1^2 c_f$. The coefficient distant from the edge will be written $c_{f\infty}$. Experimental values of $c_f/c_{f\infty}$, obtained from hot-wire measurements close to the plate, are shown in figure 4. The points are fitted closely for laminar flow by the empirical functions (accurate to $\pm 10\,\%$ S.D.)

$$c_f/c_{f\infty} = 1{\cdot}53(z/\delta_\infty)^{-\frac{1}{3}}, \quad 0 < z/\delta_\infty < 2,$$
$$= 0{\cdot}78 + 0{\cdot}84\delta_\infty/z, \quad 1{\cdot}3 < z/\delta_\infty < 4.$$

Defining the excess friction factor

$$K = \int_0^\infty (c_f/c_{f\infty} - 1)\, d(z/\delta_\infty),$$

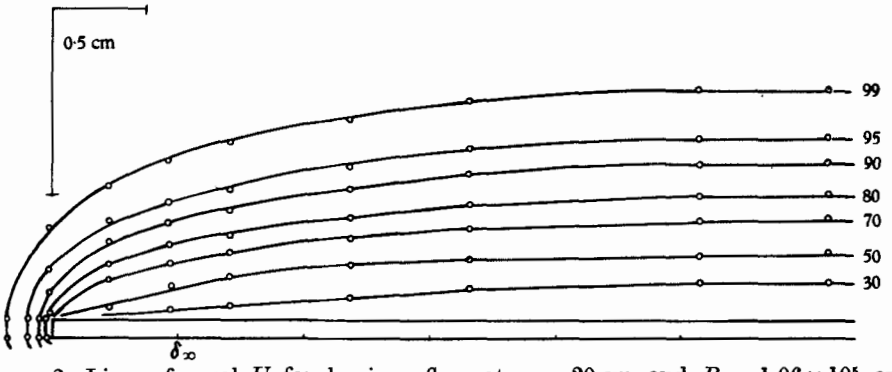

FIGURE 2. Lines of equal U for laminar flow at $x = 20$ cm and $R = 1{\cdot}06 \times 10^5$ on a flat plate. Horizontal scale $= \frac{1}{2} \times$ vertical scale. The contour values are $100\ U/U_1$.

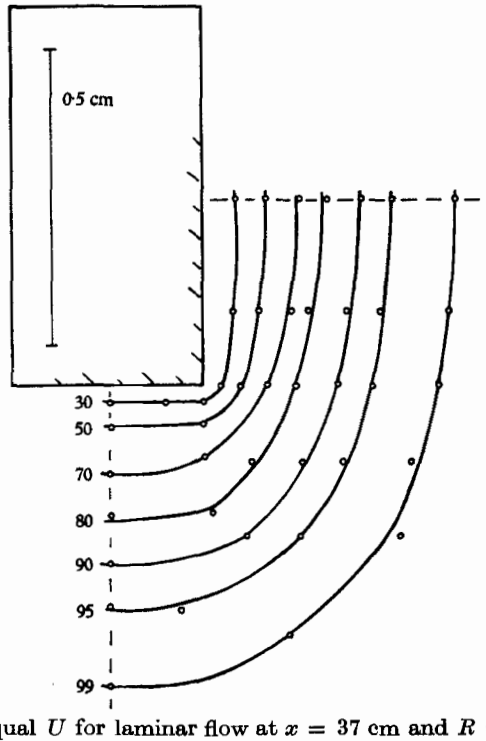

FIGURE 3. Lines of equal U for laminar flow at $x = 37$ cm and $R = 7{\cdot}2 \times 10^4$ on a rod of section 2:1 ($0{\cdot}64 \times 0{\cdot}32$ cm). The contour values are $100\ U/U_1$. Scale 1:1.

we find $K = 1{\cdot}77 \pm 10\,\%$ S.D. Alternatively, the total drag coefficient C_F is such that $(C_F - C_{F\infty})/C_{F\infty} = 53\nu x/U_1 B^2$. This value is greatly in excess of the value $K = 0{\cdot}1$ given by Howarth (1950) in his calculation based on Rayleigh's approximation. The Rayleigh approximation is clearly inadequate. On the other hand Varley's (1958) calculation gives $K = 1{\cdot}43$, only 20 % below the experimental value. This is quite good agreement.

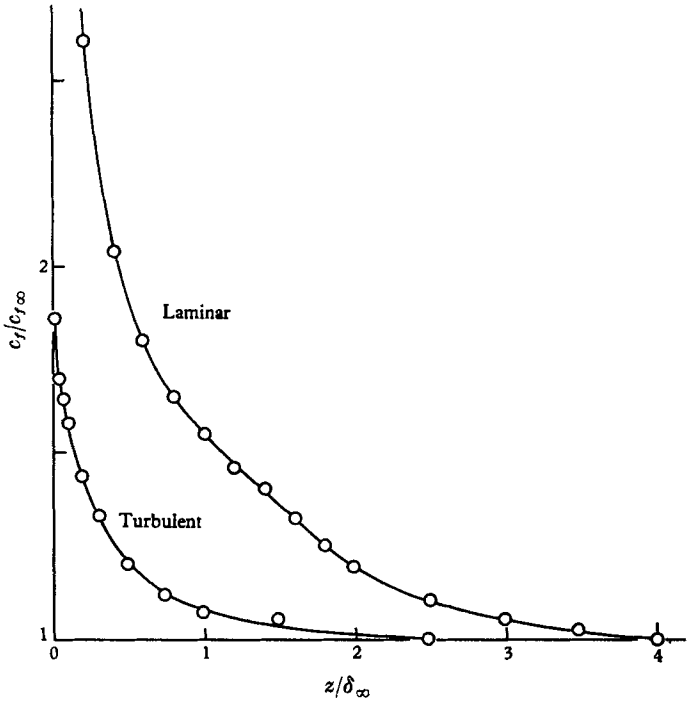

FIGURE 4. Lateral variation of laminar and turbulent skin friction on a flat plate. The turbulent values (discussed in §5) are for a plate of width $B = 6$ cm at $x/B = 10$ and $R = 4 \times 10^5$.

The edge stress

Near the edge the stress rises and will become infinite as the thickness of the plate approaches zero. For example, consider a plate of width B for which the edge cross-section is convex and symmetrical about $y = 0$ but otherwise arbitrary. The shearing force on unit length of this plate is $\oint \mu \frac{\partial U}{\partial n} ds$, for a fluid of viscosity μ, where n, s are co-ordinates normal and tangential to the plate cross-section. This expression will be independent of n near the wall where the acceleration of fluid is negligible. Hence, using polar co-ordinates (r,θ) for the edge region, with origin at the centre of curvature corresponding to each element of the edge cross-section and with $z = 0$ corresponding to $\theta = 0, \pi$, say,

$$\frac{1}{2}\oint \mu \frac{\partial U}{\partial n} ds = \int_0^B \mu \frac{\partial U}{\partial y} dz + \int_0^\pi \mu \frac{\partial U}{\partial r} r d\theta$$

$$= \text{constant as } n \to 0.$$

Both integrals are finite so that $r\partial U/\partial r$ is a function of θ as $n \to 0$. Hence near the wall U behaves like $\log r/a$ where a is the local radius of curvature. Unless, however, $\delta \gg a$, so that the region near the wall where the acceleration of fluid is negligible is at least of extent comparable with a, U is not of logarithmic form over a significant portion of the boundary layer but rather, since $\log r/a \doteq (r-a)/a$ when $(r-a)/a \ll 1$, U is of linear form near the wall.

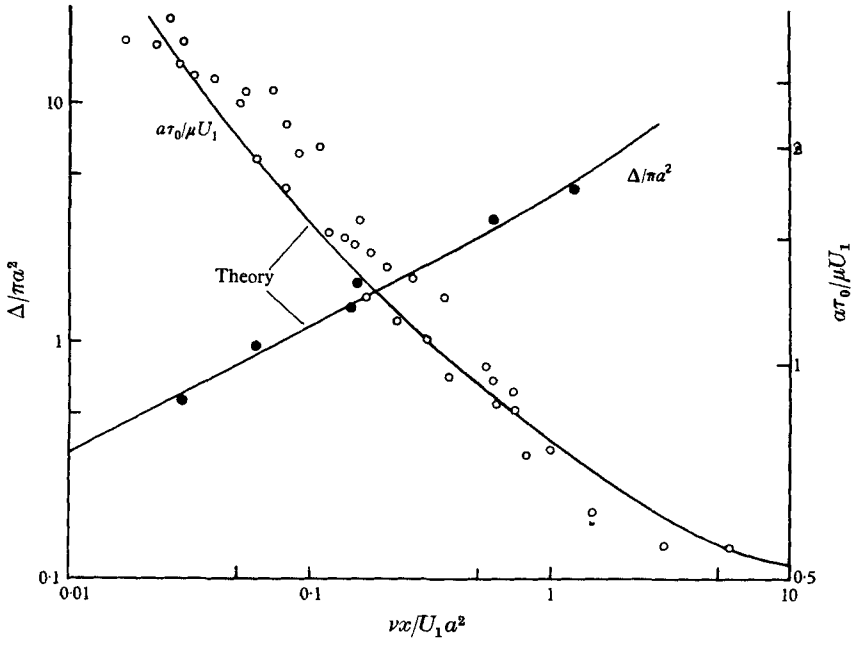

FIGURE 5. Displacement thickness Δ and skin friction τ_0 for laminar flow along a circular cylinder of radius a. Theory by Lighthill & Glauert (1955). Logarithmic scales.

It was Batchelor (1954) who first pointed out the importance of the local lateral radius of curvature in laminar flow along cylinders in his discussion of the corresponding Rayleigh problem. It should be possible to obtain an estimate of the skin friction at an edge by using the results of Lighthill & Glauert (1955) for the axisymmetric flow along a circular cylinder of radius a. Their solution is developed in terms of the parameter $(\nu x/U_1 a^2)^{\frac{1}{2}}$, proportional to the ratio of the flat plate boundary-layer thickness to the cylinder radius. They give expressions for the skin friction τ_0 and the displacement thickness

$$\Delta = 2\int_0^\infty \left(\frac{U}{U_1} - 1\right)(a+y)\,dy.$$

In order to proceed it is desirable to compare these calculations with experiment. Figure 5 compares experimental values of $a\tau_0/\mu U_1$ and $\Delta/\pi a^2$ obtained from hot-wire measurements on the circular cylinder with Lighthill & Glauert's values. The agreement to within 10–20 % is quite good so that we can now calculate the ratio of skin friction on a circular cylinder for a given $(\nu x/U_1 a^2)^{\frac{1}{2}}$ to that at the

same x on an infinite flat plate. The flat plate skin friction is given by $c_{f\infty} = 0{\cdot}664/(U_1 x/\nu)^{\frac{1}{2}}$. Typical values are shown below:

$(\nu x/U_1 a^2)^{\frac{1}{2}}$	0	1	2	5	10	20
$c_f(a)/c_{f\infty}$	1·0	2·3	3·4	6·1	9·8	16·3

Two experimental values of this ratio, accurate to $\pm 20\,\%$ S.D., were obtained. The first was for the square edge of the flat plate where $a = 0{\cdot}5$ mm, $(\nu x/U_1 a^2)^{\frac{1}{2}}$ was 3·6 and the experimental value of $c_f(a)/c_{f\infty}$ was 4·0 compared with the calculated 4·9. The second was the chamfered edge of the plate for which $a = 0{\cdot}15$ mm, $(\nu x/U_1 a^2)^{\frac{1}{2}} = 17{\cdot}6$ and the experimental value of $c_f(a)/c_{f\infty}$ was 10 compared with 14·6. This approximate agreement supports the demonstration that the viscous flow near an edge is also governed strongly by the local radius of curvature.

4. Transitional flow

The experimental results

It has been suggested that because of the comparative ease of momentum diffusion near the edge disturbances first become apparent there. This is seen in figure 6 which shows both the U-distribution and the $(\sqrt{\overline{u^2}}/U)$-distribution from measurements at $x = 51$ cm near the edge of the 20 cm plate and at two values of the Reynolds number, 1·65 and $2{\cdot}70 \times 10^5$. At $R = 1{\cdot}0 \times 10^5$ velocity fluctuations

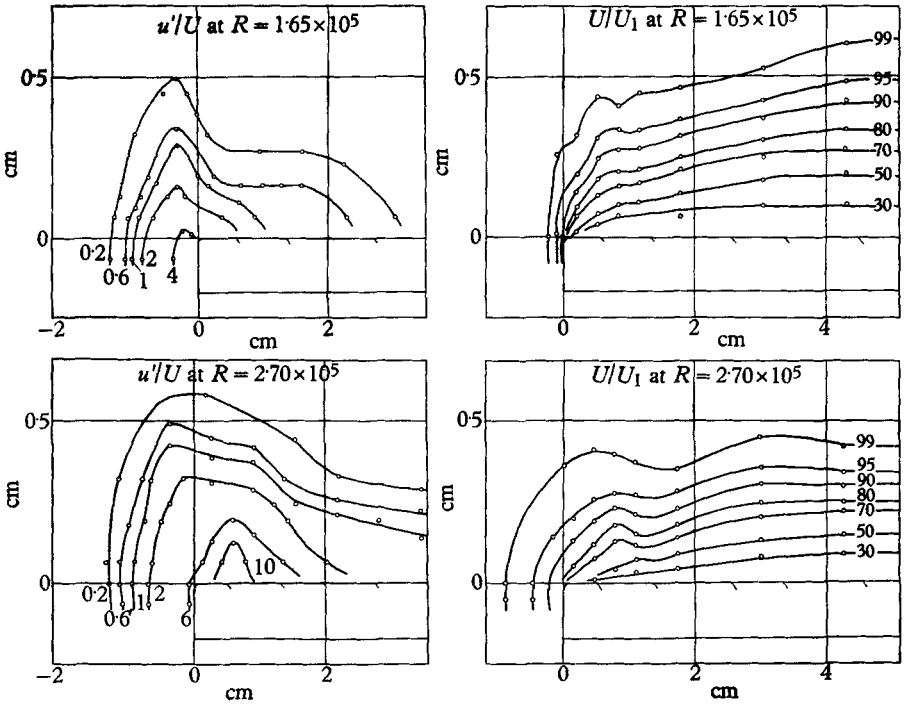

FIGURE 6. Transitional flow distributions of 100 U/U_1 and $100\sqrt{\overline{u^2}}/U$ on a finite flat plate at $x = 51$ cm, $R = 1{\cdot}65$ and $2{\cdot}70 \times 10^5$. Horizontal scale = $\frac{1}{5}\times$ vertical scale.

were barely detectable anywhere on the plate, breakdown to turbulence commenced near the edge at $R = 1{\cdot}7 \times 10^5$, and at $R = 4{\cdot}5 \times 10^5$ the whole plate was turbulent. Also it is seen that associated with the growth of the velocity fluctuations is the growth of the secondary flow discussed in §5.

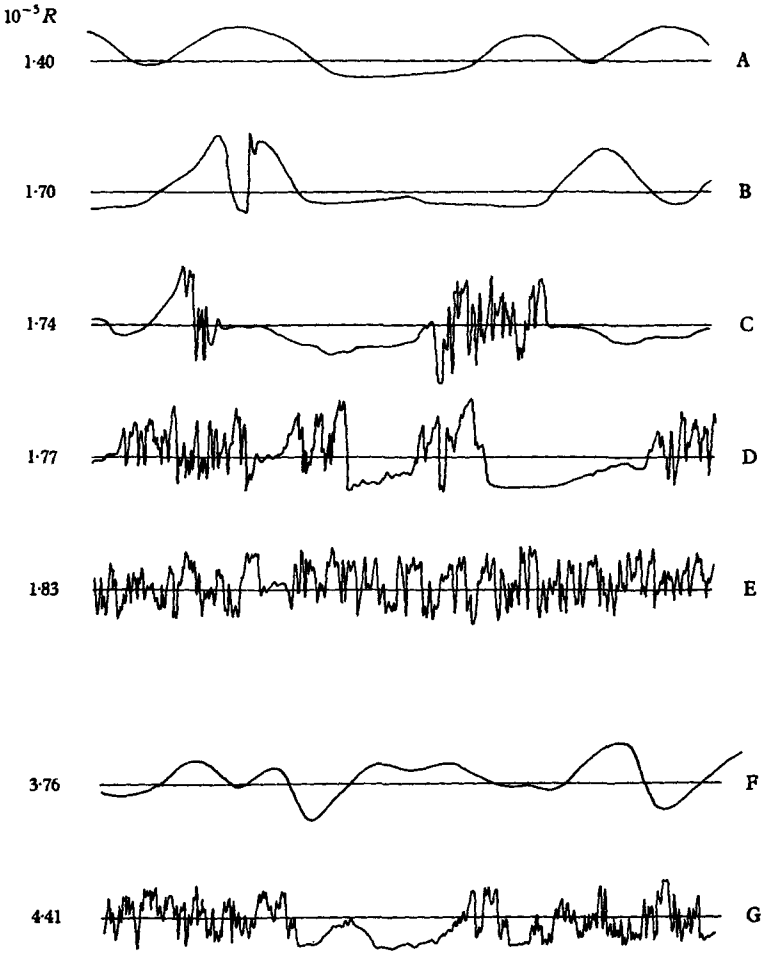

FIGURE 7. Oscillograph traces of u/U at stated values of $10^{-5}R$ and fixed sensitivity. A–E probe near the edge at (51, 0, −0·06) cm. F–G probe distant from the edge at (93, 0·06, 5·2) cm.

The character of the velocity fluctuations can be seen in portions of oscillograph traces shown in figure 7. The traces show u/U as a function of time. Traces A–E are for the probe just below the edge at (51, 0, −0·064,) cm, while traces F, G are for the probe at (97, 0·064, 5·2) cm somewhat distant from the edge. The velocity and time scales are approximately the same for all the traces. Notice that the variation of Reynolds number is obtained by varying the tunnel speed and leaving the probe fixed. Even near the edge the first fluctuations are wave-like disturbances (A). These rather irregular waves grow in amplitude until breakdown occurs (B). From these points of breakdown a turbulent region is initiated, very

small at first but growing nearly linearly in time as it is swept downstream. Two such regions, or spots, are seen in (C). As they proceed downstream the spots begin to merge (D) until the layer is swamped with spots and it is then entirely turbulent (E). Distant from the edge as in (F), (G) a similar sequence occurs, but only at a much higher Reynolds number.

Thus near the edge there is a narrow tongue of disturbed fluid while the bulk of the boundary layer remains relatively undisturbed. Within this tongue transition is obtained by the growth of turbulent spots; spots which are in every way similar to spots hitherto studied on a wide flat plate. It should be noted that spots are characteristic of transition near a wall regardless of the wall cross-section. For example, it was demonstrated both in the wind tunnel and the water channel that turbulent spots are also present during transition in the axisymmetric flow along a circular cylinder. Further, the rate at which the tongue of disturbed fluid encroaches on the surrounding boundary layer can be estimated from the oscillograph traces by reading off the intermittency factor γ, the proportion of time the fluid is turbulent. For example, in trace C, $\gamma = 0{\cdot}27$ and in trace E, $\gamma = 0{\cdot}99$. It is then found that curves of constant intermittency, drawn in the plane of the flat plate, are nearly straight lines which make an angle of $7{\cdot}9°$ to the edge (as sketched in figure 1).

The growth of the turbulent tongue

Dhawan & Narasimha (1958) have shown that Emmons's (1951) description of a transition region in terms of overlapping turbulent spots is in excellent agreement with experiment. They deduce the remarkable fact that breakdown of a laminar boundary layer, while occurring randomly in time, commences in almost point-like areas (of extent $\ll \delta$), all of which (for a plate of infinite width) lie very nearly on a straight line normal to the flow. This immediately suggests that the breakdown responsible for the tongue of disturbed fluid occurs only at a single point—the point P of figure 1. The linear growth of the curves $\gamma =$ constant would then simply be due to the linear growth of individual spots liberated from P, but if this were the case the rate of spread of this tongue ($7{\cdot}9°$) should be similar to the rate of spread of a single spot. The rate of spread of isolated spots has already been given by Schubauer & Klebanoff (1955) as $8{\cdot}6°$ ($U_1 = 300$ cm/sec), and has been independently measured here as $8{\cdot}1°$. This is in excellent agreement with the value of $7{\cdot}9°$. Further, it was directly demonstrated by using two hot-wire probes placed in the tongue of intermittently turbulent fluid upstream of the normal transition zone that turbulence never occurred at the downstream probe without having first occurred at the upstream probe. Thus near an edge breakdown originates near a single point.

The above considerations immediately raise the problem of how the edge tongue will merge with the normal transition region on the portion of the plate distant from the edge. The question reduces to the problem of the interaction of two spots as they grow and merge into one another. In a subsequent paper it will be shown that the area of a plate which is turbulent at any moment is simply the sum of the areas covered by the turbulent spots if each spot grows independently of its neighbours. There are thus two possible forms, sketched in figure 8,

of the transition curve on a plate of finite width. When the disturbance level in the free stream is low (generally at low U_1) the edge transition regions will have overlapped before normal transition occurs. At higher disturbance levels the normal transition region will have moved sufficiently upstream so that both transition regions are present.

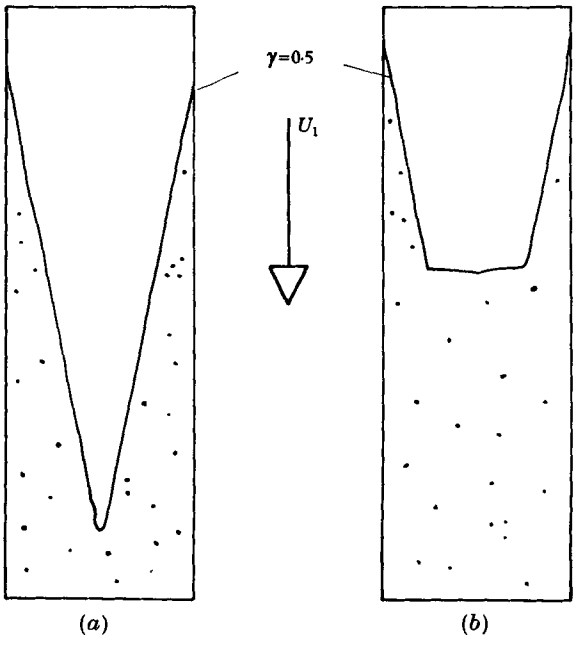

FIGURE 8. A sketch of the transition curve on a finite plate for (*a*) low and (*b*) high free-stream turbulence.

5. Turbulent flow

The secondary flow

Figures 9 and 10 show the distribution of U on a plane x = constant, based on measurements made with the 1 mm total head tube at $x = 97$ cm, $R = 8{\cdot}7 \times 10^5$ for the flat plate of figure 9 and at $x = 92$ cm, $R = 6{\cdot}7 \times 10^5$ for the 2:1 rod of figure 10. The most obvious features, as distinct from the corresponding laminar flows shown in figures 2 and 3, are that the lines of constant U are no longer everywhere convex and that the boundary-layer thickness at the edge is $1{\cdot}28\delta_\infty$ whereas in the laminar flow it was only $0{\cdot}35\delta_\infty$. The distortion of the U-distributions near the edge is strongly suggestive of a secondary flow of Prandtl's second kind in which the flow is produced by the anisotropic Reynolds stresses. But before this can be asserted it is necessary to dispose of the other possibilities. Could the secondary flow be due to the vortex found near the edge of a finite plate which is producing lift because of some error of alignment? First, the flow was symmetrical about $y = 0$. This was directly verified. The lifting vortex is found on one side only and does not therefore produce a symmetrical field. Secondly, the secondary flow is found only when the flow is turbulent whereas a lifting plate has an edge vortex even in laminar flow. This query may be put

even more generally. Is the secondary flow already present in the laminar flow? The U-distribution for laminar flow was always everywhere convex. Thus the explanation of the secondary flow is to be found in the behaviour of the turbulent layer.

A direct demonstration that the secondary flow is due to the Reynolds stresses is obtained with the vortameter, which gives the secondary flow vorticity. The vortameter did not rotate in the laminar field, but immediately transition commenced the vortameter began to rotate. At the same time the U-distribution was no longer everywhere convex. The vortameter readings were anti-symmetric about $y = 0$ and the departures from convexivity developed through the transition region. These phenomena were found for the 30, 22, 6 cm plates and the 12:1 and 2:1 rods so that the phenomena cannot be ascribed to a chance configuration of a single plate.

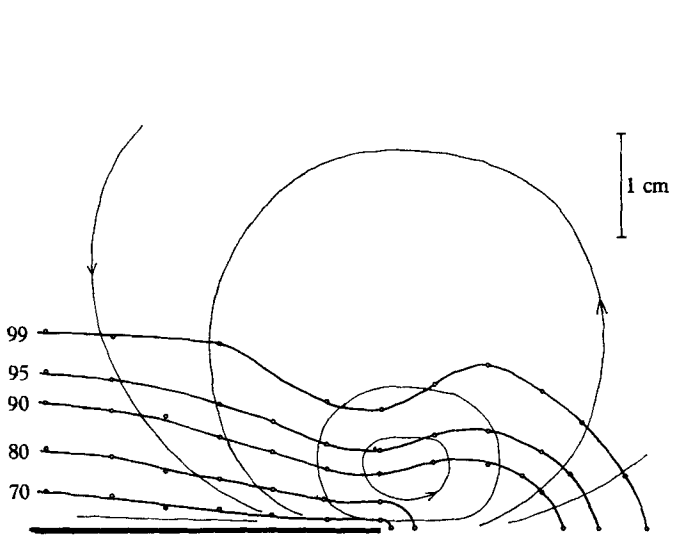

FIGURE 9

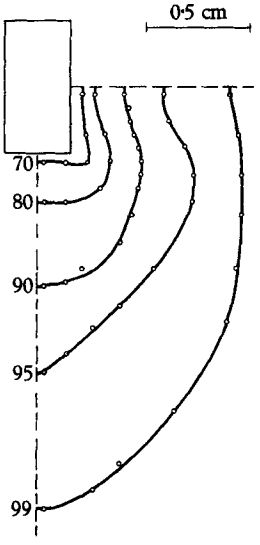

FIGURE 10

FIGURE 9. U-distribution for turbulent flow on a flat plate. Scale 1:1, $B = 30$ cm, $x = 97$ cm, $R = 8{\cdot}7 \times 10^6$. The fine lines are the secondary flow streamlines. Compare with figure 2. The contour values are 100 U/U_1.

FIGURE 10. U-distribution for turbulent flow on the rod of section 2:1. Scale 1:1, $x = 92$ cm, $R = 6{\cdot}7 \times 10^6$. Compare with figure 3. The contour values are 100 U/U_1.

The secondary flow has been measured with the vortameter for the flow of figure 9. The vortameter rotational frequency n measured in c/s is proportional to the vorticity. The secondary vorticity distribution is shown in figure 11. Notice that not only is the distribution symmetrical about $y = 0$, it is also very nearly symmetrical about a line $z = -0{\cdot}5$ cm $= -0{\cdot}017B$. The flow is such that near the wall fluid is moving away from the plate. A linear relation was found between U_1 and the frequency n at fixed x of the form $\Delta U_1 = 126\Delta n$ and such that $n = 0$ when the transition point is at x. This shows that the mean secondary vortex can be considered to be of constant pitch $= 126$ cm $= 4{\cdot}2B$. Because such

a simple relation exists between U_1 and n it is possible to replace n by the secondary flow stream function ψ defined by

$$\left(\frac{\partial^2}{\partial y^2}+\frac{\partial^2}{\partial z^2}\right)\psi = 4\pi n. \tag{5.1}$$

The stream function has been evaluated from (5·1) and experimental values of n by a relaxation calculation and is shown in figure 12. The stream function has also been drawn in figure 9 (fine lines) where the region outside $\psi/\psi_{\max} = 0{\cdot}2$ has been drawn, taking into account both the calculated values of ψ and the experimental determination of the inclination of the secondary flow vector by means of the observed inclination of a very light vane. The bulk of the secondary flow

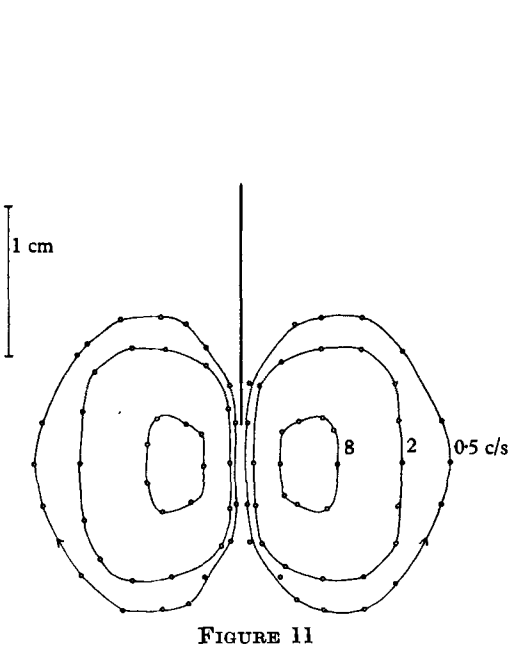

FIGURE 11

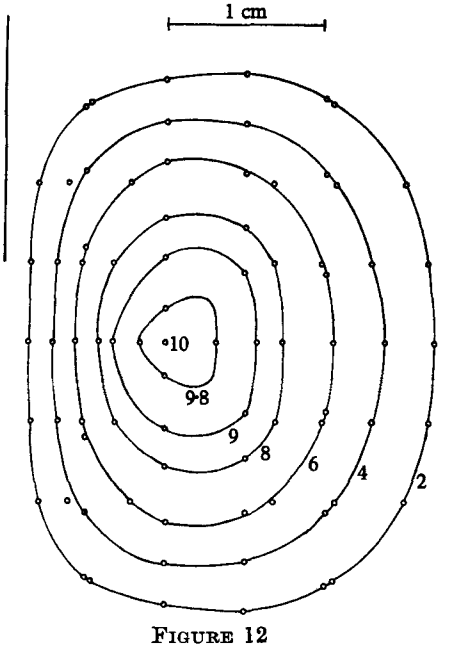

FIGURE 12

FIGURE 11. Secondary flow vorticity distribution n in c/s, near an edge. Maximum value = 8·8 c/s. B = 30 cm, x = 97 cm, $R = 8{\cdot}7 \times 10^5$. δ = 1·9 cm.

FIGURE 12. Secondary flow stream function ψ of (5·1) normalized to a maximum value of 10.

is seen to be confined to a region of dimensions δ near the edge. From ψ the secondary velocity is easily found. In figure 13 I show the maximum outflow $W = -\partial\psi/\partial y$ evaluated on the line of symmetry $z = -0{\cdot}5$ cm. W is everywhere $< 0{\cdot}037U_1$, so that in fact the secondary flow is quite small.

It would be possible to consider the mean secondary flow from two idealized points of view. First, it could be considered as a vortex, that is a small region of rotational flow outside of which the mean flow is irrotational. If this idea was completely correct the vane would have reversed its direction of rotation as it was moved into the core. In fact as shown in figure 8 such is not the case. Secondly, the secondary flow could be considered as a strong outflow near the wall and a

diffuse inflow over a large portion of plate. This idea also is not borne out by the form of ψ. In fact, ψ shows that the flow is somewhere between the two. Nevertheless, it is important to remember here that the vane was of finite size; a 1·0 cm square. Because of the finite size of the vane it may be argued that the explanation of the unidirectional rotation either side of $y = 0$ is in fact due to a strong outflow at the wall into which the vane is dipping. This assertion is clearly incorrect since the rate of rotation was extremely small even at $z = 0{\cdot}3\delta_\infty$ with the vane almost touching the wall. ψ will certainly need correction due to the finite size of the vane, but unfortunately it is rather difficult to see how this might be done.

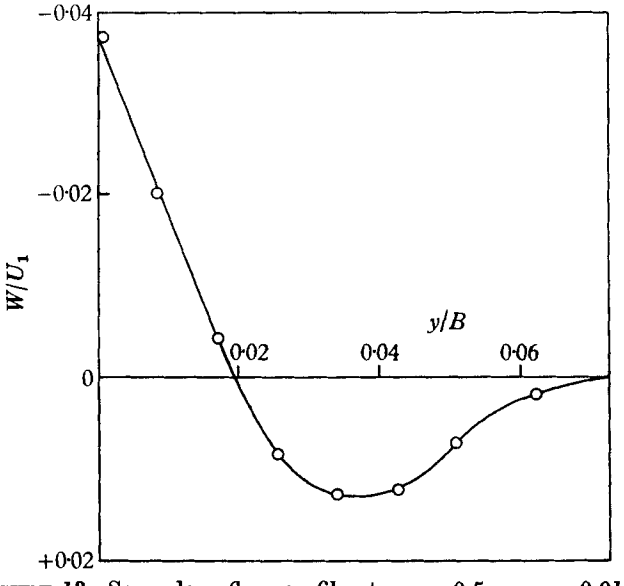

FIGURE 13. Secondary flow profile at $z = -0{\cdot}5$ cm $= -0{\cdot}017B$.
Figures 9, 11, 12, 13 are all for the same flow.

The total drag

Although there is considerable empirical data in the literature on the drag of flat plates, by far the most valuable is that due to Hughes (1954) who proposed an empirical relation for the total drag coefficient C_F of a wide plate of length L and breadth B over the range $R = 0{\cdot}04$ to 250×10^6

$$C_F = 0{\cdot}066\,(-2{\cdot}03 + \log_{10} R)^{-2}(1 + rL/B). \tag{5.2}$$

His data provides overwhelming evidence to support this dependence of C_F on R but the choice of the so-called form factor $1 + rL/B$ is unsatisfactory as the coefficient r varies strongly with both L/B and the Reynolds number $U_1 B/\nu$. It was, in fact, the need to clarify the behaviour of this factor that started the present investigation.

Figure 14 shows the distribution of skin friction obtained with a surface tube near the corner of a finite flat plate of breadth 22 cm at fixed wind speed 1050 cm/sec. The forward edge was square so that transition occurred at $x = 2$ mm, $R = 1300$ in the separated zone of extent 1·1 cm near the edge. The skin friction

rises rapidly from the line of reattachment marked $c_f = 0$ in figure 14 and except for a complex region in the corner $0 < x/B < 2$, $0 < z/B < 0{\cdot}1$ shows the gradual increase towards the side edge already shown for comparison with the laminar case in figure 4 and shown in more detail in figure 15. Note that $c_{f\infty}$ is the skin-friction coefficient for $z = \frac{1}{2}B$. Near the leading edge the behaviour is complex with at first two maxima, both displaced from the edge, then a single maximum displaced from the edge, and for $x/B > 2$ ($R < 3{\cdot}10^5$) a monotonic increase of skin

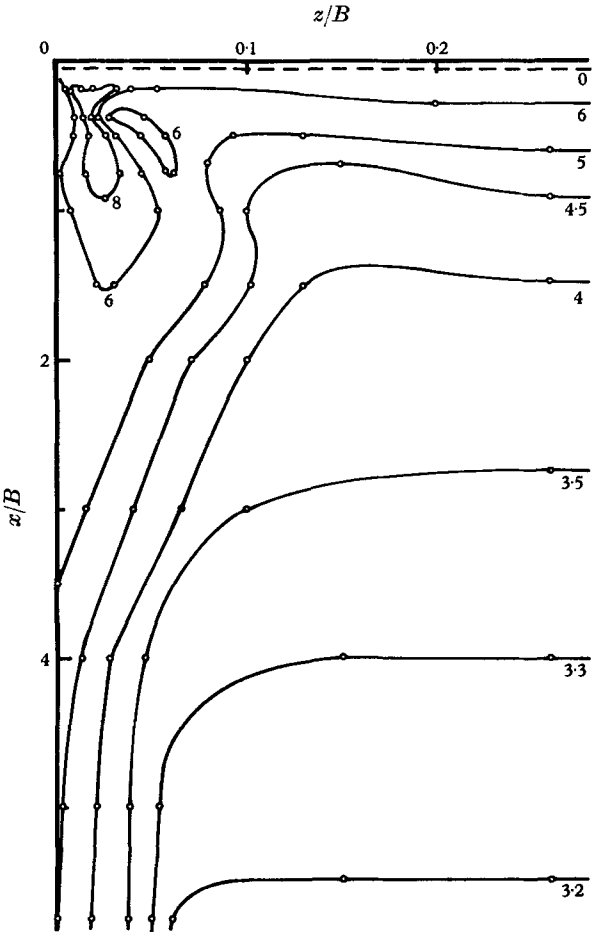

FIGURE 14. Distribution of skin-friction coefficient $10^3\, c_f$ near the corner of a finite flat plate at fixed U_1. $B = 22$ cm, $U_1 B/\nu = 1{\cdot}55 \times 10^5$.

friction to a maximum at the edge where $c_f(0)/c_{f\infty} \doteqdot 1{\cdot}8$ (much smaller than the laminar value). Included on the curve for $x/B = 3$ is the corresponding data for the 6 cm wide plate at $x/B = 10$. The close similarity of the data from the two plates shows that the lateral distribution of c_f is determined by x/B rather than x/δ as it is in the laminar case. Further downstream when δ is comparable with B the variation of c_f is less pronounced and this is illustrated also in figure 14 for $x/B = 20$ on the 2 cm wide plate.

The distribution of skin friction $c_{f\infty}$ along the centre line is shown in figure 16 for two plates of width 6 and 22 cm. Included in figure 16 is $c_{f\infty}$ obtained from

$$\left.\begin{aligned} c_{f\infty} &= R\,dC_{F\infty}/dR, \\ \text{where} \qquad C_{F\infty} &= 0{\cdot}0624\,(-2{\cdot}03+\log_{10}R)^{-} \end{aligned}\right\} \tag{5.3}$$

an expression of similar form to (5·2) but in which the coefficient 0·066 has been replaced by $0{\cdot}0624 \pm 0{\cdot}2\,\%$ S.D. This high accuracy does not refer to the absolute

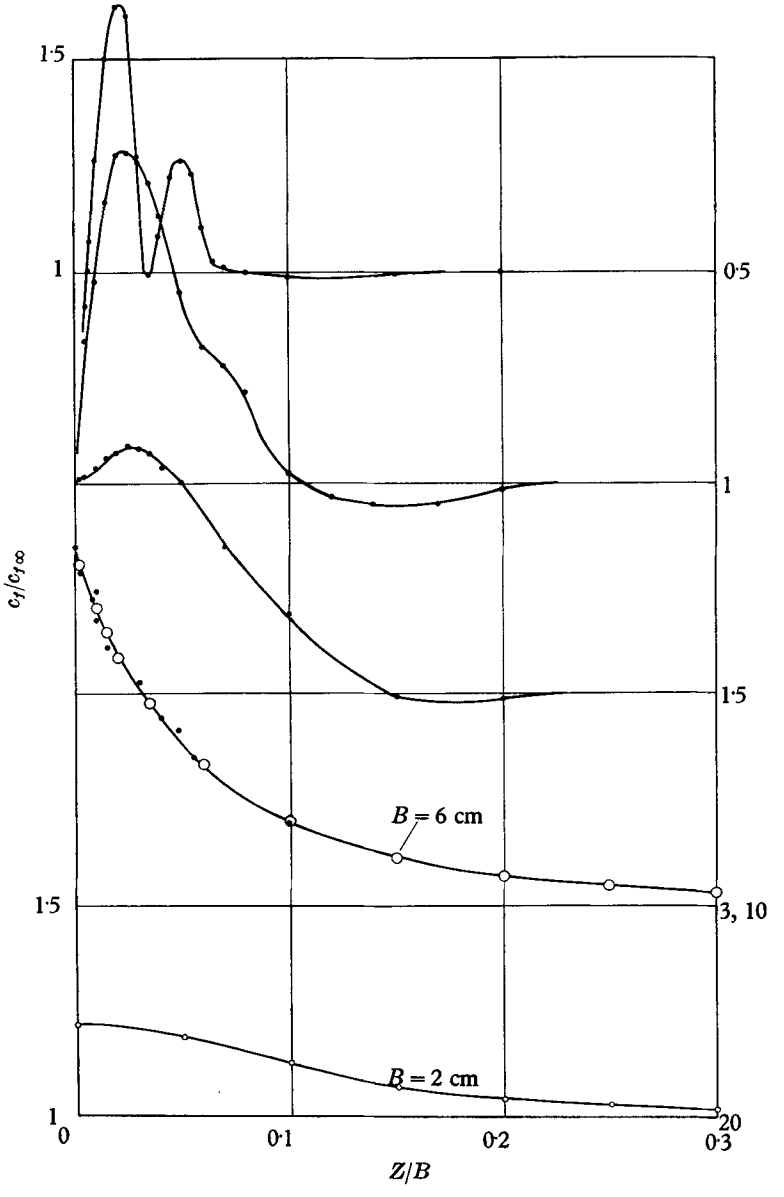

FIGURE 15. Lateral distribution of c_f at values of x/B stated on the right-hand side of the figure. $U_1 = 1050$ cm/sec. •, $B = 22$ cm, $x/B = 0{\cdot}5$, 1, 1·5, 3 (data of figure 14); ○, $B = 6$ cm, $x/B = 10$; ∘, $B = 2$ cm, $x/B = 20$.

accuracy of the coefficient but to the internal consistency of 14 separate determinations of the coefficient over the range $R = 5{\cdot}10^4$ to $5{\cdot}10^5$ for both the 6 and the 22 cm plates. (6 values from the 22 cm plate gave $A = 0{\cdot}0622$ and 8 values from the 6 cm plate gave $A = 0{\cdot}0626$.) The high accuracy does, however, support the functional form given by Hughes for the variation with R and incidentally shows that the total head tube method of measuring skin friction is very reliable. It should be noted that the velocity and stress distribution near the edge was the same for both a square edge and one chamfered to a sharp 10° wedge.

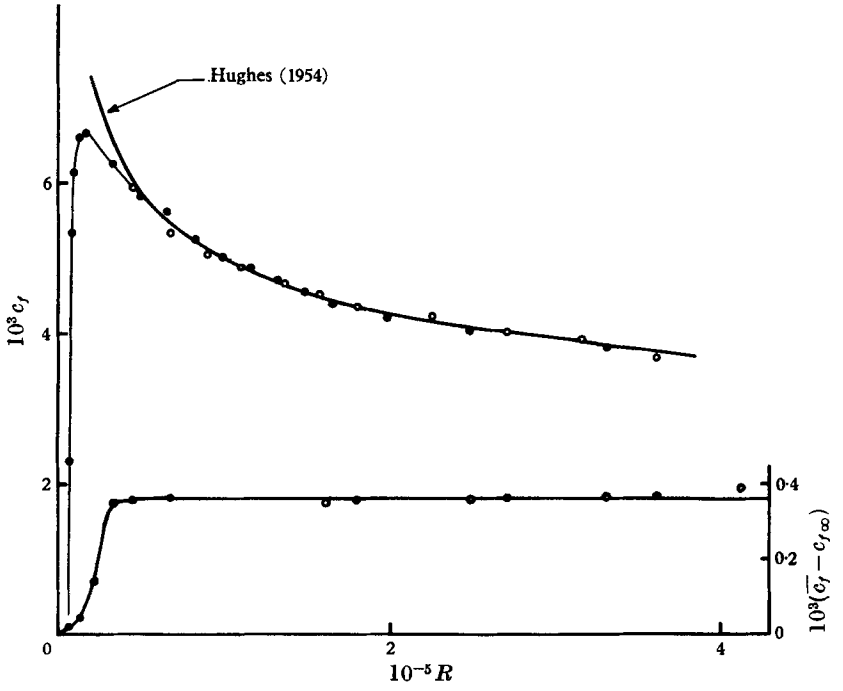

FIGURE 16. c_f along the centre line $z/B = 0{\cdot}5$ of a finite plate compared with values obtained from Hughes (1954) formula (5·3). •, $B = 22$ cm, ○, $B = 6$ cm. Also shown is the mean excess $\bar{c}_f - c_{f\infty}$. The measurements cover $0 < x/B < 10$.

Also given in figure 16 is the mean excess friction $\bar{c}_f - c_{f\infty}$ obtained by computing the mean skin friction ^{c}f with respect to z at a fixed x. As is also shown in the behaviour of $c_{f\infty}$, the influence of the leading edge is rapidly lost and the excess rises to a value independent of both R and B. This remarkable result is the key to the differences between various formulations of the drag of a flat plate. This excess will give also an increase in the total drag coefficient of a finite plate over that given by (5·3) and for the data of figure 15 this is given below.

$10^{-5}R$	0·2	0·4	0·6	0·8	1·0	1·2	1·4	1·6
$10^3\Delta C_F$	0·008	0·020	0·037	0·057	0·086	0·120	0·153	0·177

For larger values of R $\quad \Delta C_F = 3{\cdot}62 \times 10^{-4} - 30/R.$ (5.4)

The excess drag can thus be expressed as the sum of two independent contributions, one due to the finite size of the plate and arising from the flow near the side edges, the other from the particular mode of separation, transition and reattach-

ment near the leading edge. The contribution to the total drag from the leading-edge flow will be independent of x downstream of the edge region in which c_f increases rapidly so that the contribution to C_F will be of the form $-A/R$. In fact $A \doteqdot R_c[C_{FT} - C_{FL}]$, where R_c is the Reynolds number at the end of the leading-edge region, C_{FT} is the turbulent friction coefficient given by (5.3) at R_c and C_{FL} is the actual friction coefficient for the edge region. For natural transition A can easily be as large as 10^3 and through R_c is very dependent on U_1, but in the present case of transition behind a square leading edge A is almost independent of U_1 and the value $A = 30$ given by (5.4) is reasonable.

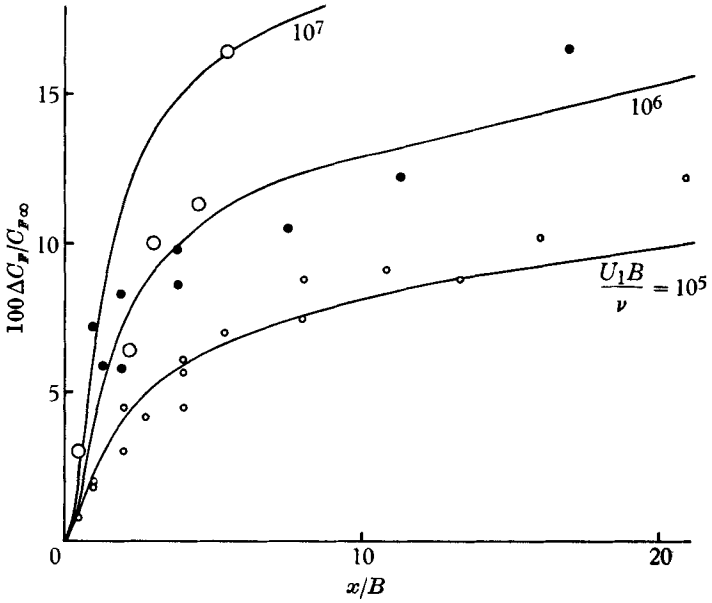

FIGURE 17. The percentage form factor for the total drag as a function of the aspect ratio at various U_1B/ν. The experimental points are given by: ○, Hughes (1954) sheet values, $U_1B/\nu = 2{\cdot}0 \times 10^5$. ●, Hughes (1954) pontoon values, $U_1B/\nu = 1{\cdot}9 \times 10^6$. ○, Allan & Cutland (1953) plank values, $U_1B/\nu = 0{\cdot}81 \times 10^7$.

The determinations of drag reported in the literature are largely for a series of runs at fixed U_1, B with variable plate length x. This data has been collected in figure 17. The curves of constant U_1B/ν are obtained from ΔC_F of (5.4) and C_F of (5.3) at $R = (U_1B/\nu)(x/B)$. The experimental data given by Hughes (1954) for plastic sheets with $U_1B/\nu = 2{\cdot}0 \times 10^5$ and pontoons with $U_1B/\nu = 1{\cdot}9 \times 10^6$ and by Allan & Cutland (1953) for planks with $U_1B/\nu = 0{\cdot}81 \times 10^7$ lie close to the appropriate curves derived from the present data. The sheet values of C_F are accurate to $\pm 1{\cdot}0\,\%$ S.D. and the pontoon values to $\pm 0{\cdot}5\,\%$ S.D. while the consistency of the measurements reported here suggests an accuracy of $\pm 0{\cdot}7\,\%$ S.D. for the total head values of C_F. Thus all this data is consistent to better than $\pm 1\,\%$ S.D.

A number of semi-empirical relations have been given (Schlichting 1955) for C_F, of which the theoretically soundest is that due to Townsend (1956)

$$\sqrt{2}\,kC_F^{-\frac{1}{2}}(1 - R_0/R)^{\frac{1}{2}} = \log RC_F + 1{\cdot}1, \tag{5.5}$$

where $k = 0{\cdot}41$ is the logarithmic velocity profile constant, R_0 is a constant of integration and 1·1 is an empirical constant obtained from the known velocity distribution. If $R_0 = 0$ and the 1·1 is ignored, (5·5) is similar to the widely used Schoenherr (1932) relation

$$0{\cdot}242C_F^{-\frac{1}{2}} = \log_{10} RC_F. \tag{5.6}$$

The experimental constant 0·242 corresponds to $k = 0{\cdot}394$, considerably different from the accepted value 0·41. As values of C_F are sensitive to the choice of this coefficient (5.6) must be regarded simply as an empirical relation. Schoenherr's data were obtained from the total drag of finite plates and no attempt was made to allow for the effect of aspect ratio. But since by (5.4) the effect of the aspect ratio is merely to increase the drag coefficient by an almost constant amount so that the drag is almost independent of the aspect ratio, then Schoenherr's relation or any other empirical relation obtained by ignoring the effect of aspect ratio should give a good estimate of the total drag of any finite plate. Values given by Schoenherr's relation exceed those of (5.3) by $(1{\cdot}0, 4{\cdot}5, 4{\cdot}1, 3{\cdot}2, 2{\cdot}6) \times 10^{-4}$ at $R = (10^5, 10^6, 10^7, 10^8, 10^9)$, while for the Prandtl–Schlichting relation (Schlichting 1955)

$$C_F = 0{\cdot}455/(\log_{10} R)^{2{\cdot}58}, \tag{5.7}$$

the corresponding values are $(0{\cdot}8, 5{\cdot}1, 4{\cdot}8, 3{\cdot}8, 3{\cdot}2) \times 10^{-4}$. These differences follow quite closely those given by (5.4) with discrepancies in the various values for C_F generally much less than 10^{-4} and certainly not more than the experimental error of rather less than $\pm 1\,\%$ S.D.

In estimating the drag of ship-like bodies the values of C_F given in (5.3) can be used with confidence but due to the presence of a free surface or a keel of large angle the excess friction ΔC_F may differ from (5.4). However, the presence of a free surface does not appear to affect ΔC_F, since the results of Allan & Cutland (1953) who used a semi-submerged plank are consistent with all the other data presented here. The effect of the keel angle on ΔC_F could be obtained by local skin-friction measurements with the surface tube on a body made of two equal finite flat plates at zero incidence and touching each other along an edge.

It should be noted that (5.4) contains a contribution to the drag independent of viscosity. This result was, however, obtained by measurements only up to $R \doteqdot 10^6$ and in spite of being in good agreement with published results up to $R \doteqdot 10^9$ is entirely empirical. It cannot be used with confidence outside the limits of the original data, $R = 10^4$ to 10^9 and in particular cannot contribute to the question of whether or not the drag coefficient of a finite plate at $R = \infty$ is zero or finite. In practice large values of R can only be achieved at large values of δ/B so that the question of drag at $R = \infty$ is best answered by studies of the flow along a long thin wire.

The result that ΔC_F is independent of B is surprising for it may have been supposed that provided B is sufficiently large for the two edge flows not to interact then the contribution of the edge flow to ΔC_F would be of the form (constant)/B. The data clearly show that this is not so, and the edge flows must interact for all values of B. A comparison of the lateral distribution of c_f on the 6 and 22 cm wide plates at $x/B = 10$, 3, respectively, as already given in figure 15 shows that while the rise of c_f at the edge is much the same in the two cases the lateral extent of the

excess edge friction is less for the narrower plate. It is unexpected that in spite of this interaction $c_{f\infty}$ is unaffected. Nevertheless, $c_{f\infty}$ will be affected when the plate is sufficiently narrow for the edge flows to overlap. Any effect is small since the values of A determined from the 6 and 22 cm plates were 0·0626 and 0·0622 with a barely significant difference of 0·7%, while the value obtained from a 2 cm wide plate 0·0600 is still only 2·4 % below the value for a wide plate.

I gratefully acknowledge that my period of research at Cambridge was made possible by my employers, the New Zealand Defence Scientific Corps. Some of the material presented here was described by Dr A. A. Townsend (1958) at the Freiburg symposium on boundary-layer research.

REFERENCES

ALLAN, J. F. & CUTLAND, R. S. 1953 *Trans. N.E.C. Inst.*, p. 245.
BATCHELOR, G. K. 1954 *Quart. J. Mech. Appl. Mech.* **7**, 179.
CHARTERS, A. C. 1943 *N.A.C.A.* TN 891.
DHAWAN, S. & NARASIMHA, R. 1958 *J. Fluid Mech.* **3**, 418.
EMMONS, H. W. 1951 *J. Aero. Sci.* **18**, 490.
HOWARTH, L. 1950 *Proc. Camb. Phil. Soc.* **46**, 127.
HUGHES, G. 1954 *Trans. Inst. Naval Arch.* **96**, 314.
KLEBANOFF, P. S. 1954 *N.A.C.A.* TN 3178.
LIGHTHILL, M. J. & GLAUERT, M. B. 1955 *Proc. Roy. Soc.* A, **230**, 188.
MOORE, F. K. 1956 *Advanc. appl. Mech.* **4**, 159.
MURPHY, J. S. & PHINNEY, R. E. 1951 *J. Aero. Sci.* **18**, 771.
PRANDTL, L. 1952 *Essentials of Fluid Dynamics.* London: Blackie.
PRESTON, J. H. 1954 *J. Aero Sci.* **21**, 109.
RAYLEIGH, LORD 1911 *Phil. Mag.* (6) **21**, 697.
SCHLICHTING, H. 1955 *Boundary Layer Theory.* London: Pergamon Press.
SCHOENHERR, K. E. 1932 *Trans. S.N.A.M.E.* **40**, 279.
SCHUBAUER, G. B. & KLEBANOFF, P. S. 1955 *N.A.C.A.* TN 3489.
TAGORI, T. *et al.* 1955 *J. Soc. Nav. Archit. Japan*, **98**, 31.
TOWNSEND, A. A. 1954 *European Shipbuilding*, **3**, 86.
TOWNSEND, A. A. 1956 *The Structure of Turbulent Shear Flow.* Cambridge University Press.
TOWNSEND, A. A. 1958 *Boundary Layer Research.* Proc. Freiburg symposium. Ed. H. Görtler. Berlin: Springer-Verlag.
TRUITT, R. W. 1956 *J. Aero. Sci.* **23**, 889.
VARLEY, E. 1958 *J. Fluid Mech.* **3**, 601.